Journal of Power Sources 556 (2023) 232504

Contents lists available at ScienceDirect

Journal of Power Sources

journal homepage: www.elsevier.com/locate/jpowsour

Test procedure for the prediction of water transport in polymer electrolyte fuel cells

Lukas Lübben [a,c,b], Sebastian Kirsch [a], Thomas Kadyk [b,d], Michael Eikerling [b,c,d,*]

[a] Volkswagen AG, Am Krainhop 5, 38550 Isenbüttel, Germany
[b] Theory and Computation of Energy Materials (IEK-13), Institute of Energy and Climate Research, Forschungszentrum Jülich GmbH, 52425 Jülich, Germany
[c] Chair of Theory and Computation of Energy Materials, Faculty of Georesources and Materials Engineering, RWTH Aachen University, 52062 Aachen, Germany
[d] Jülich Aachen Research Alliance, JARA Energy, Jülich, Germany

HIGHLIGHTS

- Semi-empirical water transport model, parametrized with measurement data.
- Computationally efficient prediction of channel-to-channel water fluxes.
- Advanced calculation of operating condition profiles.
- Reliable test procedure for water transfer measurements.

ARTICLE INFO

Keywords:
PEM fuel cell design
Water management
Water crossover
Quantitative prediction

ABSTRACT

Water plays a crucial role for the operation of polymer electrolyte fuel cells. The distribution and state of water in the membrane-electrode-assembly (MEA) not only impacts the performance of the cell, but also its degradation and freeze-start capability. It is therefore important to have a model that precisely predicts the distribution of water across the fuel cell for arbitrary inlet conditions. Unfortunately, water transport coefficients reported in the literature vary by orders of magnitude while operation conditions and other crucial properties of the cell are not precisely known. Furthermore, a large amount of data is simply outdated due to improvements in measurement techniques and setups as well as fuel cell components. In the present work, we have devised a test procedure for water transfer measurements with state of the art MEAs. In parallel, we have derived a semi-empirical model and parametrized it with measured data. The model allows predicting MEA water fluxes and profiles of temperature and concentration over a wide operation range, relevant for passenger as well as heavy duty automotive applications.

1. Introduction

For the operation of polymer electrolyte fuel cells (PEFCs), water plays a crucial but double-sided role as both active reaction medium and asphyxiant, that blocks gas transport. Water is generated inside the PEMFC as the product of the oxygen reduction reaction (ORR). Additionally, it is brought into the cell with humidified reactant gases. Its distribution across the functional porous electrode layers does not only impact the performance, but also has implications for lifetime, cost, reliability and safety. Overall, the optimal water content is determined by the interplay of opposing trends [1,2]. If the cell water content is too low, the proton conductivity is reduced [1,3] and resistive losses as well as ionomer degradation are accelerated [4]. On the other hand, if flooding of porous layers are too high, O_2 transport is impeded, causing performance losses [5–7] and accelerated degradation of the cathode electrode as Pt dissolves more easily at higher humidity [8]. If flooding affects the anode, fuel starvation and resulting carbon corrosion on the cathode can occur, also reducing lifetime [9]. Additionally, residual water and its distribution across the cell causes a tremendous impact on the freeze-start capabilities of the cell [10]. Therefore, it is important to have a model that accurately predicts the distribution of water across the fuel cell for arbitrary inlet conditions and specific for the MEA type of interest. Hereby, we explicitly consider the GDLs as a part of the MEA.

The literature is rich in water transport models as collected in a number of reviews [2,3,11–14]. The most common macroscale transport models are based on the approaches of Springer et al. [15], Bernardi and Verbrugge [16] as well as Fuller and Newman [17]. The first two models are isothermal, stationary and one-dimensional

* Corresponding author.
E-mail address: m.eikerling@fz-juelich.de (M. Eikerling).

https://doi.org/10.1016/j.jpowsour.2022.232504
Received 29 September 2022; Received in revised form 1 December 2022; Accepted 6 December 2022
Available online 16 December 2022

in through-plane direction. But they differ in the way the driving forces are defined. While the Springer model ascribes the flux of water to two factors, namely diffusion and electroosmotic drag, the model of Bernardi and Verbrugge is based on hydraulic permeation. The model of [17] was derived from concentrated solution theory and also considered effective heat transfer. This model suffers from two aspects. Firstly, it neither considers water condensation in porous layers nor liquid water transport. Secondly, the required parameters are difficult to determine in experiments that closely mimic the conditions of application. Hence, the prevailing approaches are still based on diffusion [18] and hydraulic permeation models [19] or combinations thereof [20–22].

Numerous groups have focused on describing water transport through the membrane as a function of membrane water content λ, a relation that can be derived from adsorption isotherms measured *ex situ* [23]. Thereby, the experiments are carried out with water vapour or liquid. However, fully saturated water vapour or liquid water have an activity of one, but cause different λ [3]. This phenomenon known as Schröder's paradox was resolved by Eikerling and Berg in [24]. Considering that a portion of electrode pores in contact with the membrane is flooded due their hydrophilic nature [1], water transport predictions in fuel cells will be incorrect if they do not different between flooded and unflooded pores. Also, continuous through-plane descriptions of temperature and concentration profiles are often absent, which represents an oversimplification if consistent predictions over a wide range of operating conditions are needed.

A model specifically focusing on the determination of these profiles was published by a group at General Motors [5,25]. The purpose of the model was to explain the origin of cathodic mass transport losses caused by GDL flooding. The model is based on the calculation of through-plane temperature and concentration profiles across the cathode and was parametrized using limiting current density measurements as well as thermal conductivities of the cell components. Furthermore, design aspects of flow fields were incorporated. The model accounts for through-plane vapour transport and how it depends on heat and mass transport properties of the GDL as well as operation conditions in the flow field channel. It can be used to determine the relative humidity in the cathode catalyst layer as well as at the membrane interface. As humidity is a key stressor for the degradation of membrane and electrodes, the model is a sound basis for studies of lifetime aspects. However, the problem with the GM model is that it neither treats water transport through the membrane nor the anode properly. The total water flux at the membrane catalyst interface is simply fixed. To recapture the cathode water pressure profiles at various sets of operating conditions it is therefore needed that this boundary condition is identified for any set. Of course the total water flux is also influenced by the membrane thickness [26] as well as the GDLs [27,28].

In parallel to the modelling works, several experimental setups and measurement techniques for the assessment of membrane water transport have been presented in the literature, using PEFC single cells [29–34], PEFC stacks [35,36] or *ex situ* techniques [26,37,38]. While stack-based experiments try to realistically map the system behaviour, *ex situ* measurements are used specifically for the analysis of fundamental, isolated mechanisms. In contrast, single differentially operated cells are particularly suitable to investigate the effects of operating conditions in the channel, while being still close to the application.

In this paper, we lift restrictions of existing models by integrating water transport through the membrane and the anode half cell. We parametrize the model with single cell data of a dedicated membrane water transport experiment. The design of the experiment is based on precise sensors for process control as well as measurement and data are collected for a wide range of operating conditions. The model is designed to predict the water flux to the channel for a wide range of relevant operating conditions as well as the through-plane temperature and concentration profiles for the MEA under test.

2. Experimental

Experimental data were collected using a $50\,cm^2$ commercially available MEA and a straight channel flow field design. The used "Gore A510.1M735.18C580.4" MEA contains a reinforced, persulfonic acid-based membrane with a thickness of $18\,\mu m$ and a cathode with a Pt loading of $0.4\,mgPt/cm^2$. Freudenberg H15CX483 gas diffusion layers were used on both electrodes, compressed with pneumatic bladder hardware from Greenlight Innovation Inc. to an average GDL-compression of $1\,MPa$ in the active area.

Net water flux

Electrochemical data and operating conditions were gathered with a fully automated single-cell test station from Horiba FuelCon using Michell Instruments dew point sensors (Optidew 501) and an additional external potentiostat (Zahner Zennium), as depicted in Fig. 1, to determine the *in situ* water flux. The water content in the gas inlet and outlet of the cell was determined and a balance equation established. To measure the water content in the inlet or outlet gas, capacitive/ohmic sensors [39,40] or infrared [35], spectrometry methods [41] and cooled mirrors [42] as well as water traps [29,30,33,43–46] were used. A comparison of the influences on the measurement accuracy of the different sensors is shown in Fig. 2. Most convincingly, four dew point sensors were implemented, which provide adequate load-following dynamics, accuracy and case of integration. Besides the typical test station design, we integrated two coolant loops for the control of temperatures at anode and cathode. The outlet gas tubes were heated to $5-15\,K$ above the maximum coolant temperature to evaporate all liquid water. The cell was operated in co-flow mode with constant mass flow rates (Anode $2\,nlm$, Cathode $3\,nlm$) causing a low pressure drop (Anode $< 50\,mbar$, Cathode $< 150\,mbar$) also at lowest absolute pressure of $1.5\,bara$. Furthermore, to have a direct feedback of changes in RH onto the Ohmic cell resistance, a continuous impedance measurement at $1\,kHz$ was integrated in the experimental setup.

For optimal performance and reproducibility, all test cells had undergone a break-in procedure, consisting of several step changes in current and voltage, similar to Christmann et al. [47]. During this conditioning phase, the cell was hydrated, contaminants were removed and the catalyst activity was seen to increase [48]. Water transport measurements were performed at nominal temperatures of $50\,°C$, $60\,°C$, $70\,°C$, $80\,°C$ and $1.1\,bara$, $2\,bara$ and $3\,bara$ respectively, while the nominal dew points were always $5\,K$ or more below the nominal cell temperatures, to avoid liquid water inside the cell. At each set of operating conditions, the individual driving forces for water transport (according to the model) were varied, i.e., pressures and humidities in anode and cathode, as well as the load, were altered as summarized in Table 1. Humidity and load ramping between test points were applied to keep the flow field channels and GDLs free of liquid water at any time. After a steady state high-frequency resistance is reached, the respective measurement was started. The measurement time for each test point in any set of operating conditions was $10\,min$. During this time, the operating conditions as well as the water flux are measured each second. Using cyclic voltammetry (CV) measurements, it was ensured that hydrogen crossover related water production was low enough at any time to be negligible in the water balance.

Thermal conductivity

To measure the effective steady-state through-plane thermal conductivity of the components we have used a similar *ex situ* measurement setup as employed in [49,50]: in an insulated housing a heat flux was forced through pieces of GDLs or flow fields with $4\,cm^2$ cross-sectional area. The heat flux was determined from Fourier's law of thermal conduction with the help of several temperature sensors, which were installed at defined positions along the sample holder.

Table 1
Variations in applied nominal operating conditions used to measure water flows at different driving forces.

Test point	Load	Inlet pressures		Inlet dew points	
	Current density [A cm^{-2}]	Anode [bara]	Cathode [bara]	Anode [°C]	Cathode [°C]
1	0	nominal	nominal	nom.−5	nominal
2	0	nominal	nominal	nom.−10	nominal
3	0	nominal	nominal	nominal	nom.−5
4	0	nominal	nominal	nominal	nom.−10
5	0	nom.+0.5	nom.−0.5	nominal	nominal
6	0	nom.−0.5	nom.+0.5	nominal	nominal
7	0.5	nominal	nominal	nominal	nominal
8	1	nominal	nominal	nominal	nominal
9	1.5	nominal	nominal	nominal	nominal

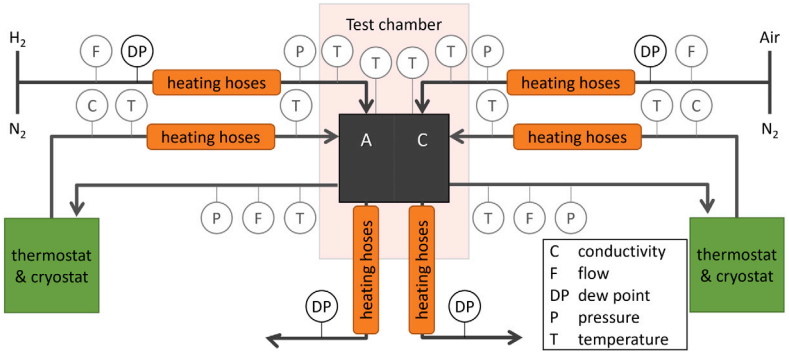

Fig. 1. Process and instrumentation scheme of the test station for water flow measurements. Equipped with four dew point sensors, a special heating concept and precise sensors for process control.

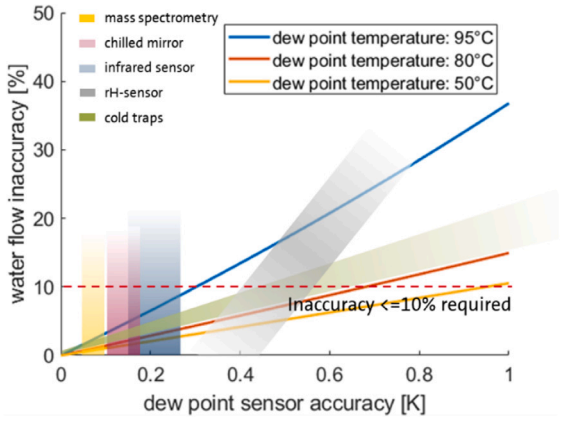

Fig. 2. Estimated accuracy of different sensor types in this specific measurement setup at $3\,nl_{dry}$ air, 1.1 bara and 5 min hold time.

Model parametrization

Experimentally recorded measurement data of the net water transport are then used to parametrize the model described in the next section. For this purpose, the Sequential Quadratic Programming (SQP) algorithm, implemented in Matlab's "fmincon" function, was used.

3. Modelling

Water transport is modelled as a one-dimension process in through-plane direction z, assuming that partial gas pressures in the channels remain constant. Thereby, the water vapour partial pressure p_{H_2O} for the inlet and outlet gas streams is calculated from the dew point measurements, using the equation of Springer et al. [15],

$$p_{H_2O} = exp(A + B \cdot T_{dp} - C \cdot T_{dp}^2 + D \cdot T_{dp}^3) \quad \text{[Pa]} \quad (1)$$

$$A = 6.50784$$

$$B = 0.067995$$

$$C = 2.11463 \cdot 10^{-4}$$

$$D = 3.2816 \cdot 10^{-7}$$

The water fluxes at cell inlet and outlet, $j_{H_2O}^{in/out}$, are calculated on the basis of the ideal gas law and the equation of state of humid air

$$j_{H_2O}^{in} = \frac{p_{H_2O}^{in}}{p^{in} - p_{H_2O}^{in}} \cdot \frac{p_{ref}}{R \cdot T_{ref}} \cdot j^{in} \quad \text{[mol cm}^{-2}\text{ s}^{-1}\text{]} \quad (2)$$

$$j_{H_2O}^{out} = \frac{p_{H_2O}^{in}}{p^{in} - p_{H_2O}^{in}} \cdot \frac{p_{ref}}{R \cdot T_{ref}} \cdot \left(j^{in} - j^{consumed}\right) \quad \text{[mol cm}^{-2}\text{ s}^{-1}\text{]} \quad (3)$$

with the total volume fluxes j^{in}, the absolute pressure $p^{in/out}$ and, in case of the cathode side, flux corresponding to the amount of gas consumed by the ORR, $j^{consumed}$. The net anode water flux, equal to the net water transport through the PEM, is given by

$$j_{H_2O,anode}^{net} = j_{H_2O}^{out,anode} - j_{H_2O}^{in,anode} \quad \text{[mol cm}^{-2}\text{ s}^{-1}\text{]} \quad (4)$$

In the PEM, physically, the water is transported due to liquid water pressure differences (also referred to as hydraulic permeation) and electro osmosis [24]. Modelling hydraulic PEM permeation requires the specification of the thermodynamic equilibria at the membrane electrode interfaces and therefore, among other variables, the modelling of the liquid pressure in the electrodes. Unfortunately, the liquid pressure in the electrodes can neither be measured directly nor simulated as the relevant properties of electrodes and GDLs i.e. resistance against liquid water flow, distributions of pore sizes and contact angles are missing in our data set. However, the liquid pressure, in the end, is a function of component properties and operating conditions. Accordingly, we specify the PEM water transport as a direct function of the operating

conditions, namely gradients in concentration, pressure, and electric potential. The through plane water pressure profile is given by

$$0 = D_{H_2O,c}(z) \cdot \frac{d^2 p_{H_2O}(z)}{dz^2} + \begin{cases} \frac{i}{2 \cdot F \cdot d_{CCL}} & CCL \\ D_{H_2O,p} \cdot \frac{d^2 p(z)}{dz^2} + \frac{n_{H_2O,i}}{F} \cdot \frac{di^+}{dz} & PEM \\ 0 & MPL\&GDL \end{cases} \tag{5}$$

with the Dirichlet boundary conditions to the ordinary differential equation (ODE)

$$p_{H_2O}(z = z|_{ch,a}) = p_{H_2O,in,anode} = p_{H_2O,sat}(T_{dp,in,anode}) \quad [Pa] \tag{6}$$
$$p_{H_2O}(z = z|_{ch,c}) = p_{H_2O,in,cathode} = p_{H_2O,sat}(T_{dp,in,cathode}) \quad [Pa]$$

where d_{CCL} describes the thickness of the cathode catalyst layer (CCL), i is the geometric current density in the CCL, i^+ (identical value as i) the geometric proton current density in the membrane. Accordingly, the water production rate in the CCL, i.e., $i \cdot (2 \cdot F \cdot d_{CCL})^{-1}$, is assumed to be homogeneous in the through-plane direction. $p_{H_2O}(z = z|_{ch,a/c})$ is the water vapour partial pressure in the channels calculated with the dew point temperatures averaged from inlet and outlet sensors. The pressure profile $p(z)$ in the PEM is considered linearly increasing from one isobaric electrode to the other. With the exception of the membrane, the water diffusion coefficient is calculated from dry porosity, ϵ_{dry}, and tortuosity, τ, of the different components (listed in Table 2), multiplied by the free diffusion coefficient $D_{H_2O}^{free}$ of the gas.

$$D_{H_2O,c}(z) = D_{H_2O}^{free} \cdot \frac{\epsilon_{dry}}{\tau} \quad [cm^2\ s^{-1}] \tag{7}$$

The transport coefficients of the membrane $D_{H_2O,c}$, $D_{H_2O,p}$ and $n_{H_2O,i}$ are fitted based on the experimental water flow data and presented in "Results and discussion". $j_{H_2O}(z)$ is the local water flux defined in the porous transport layers by

$$j_{H_2O}(z) = -D_{H_2O,c}(z) \cdot \frac{d\, p_{H_2O}(z)}{dz} + \begin{cases} 0 & CCL \\ -D_{H_2O,p} \cdot \frac{dp(z)}{dz} + \frac{n_{H_2O,i}}{F} \cdot i^+ & PEM \end{cases} \quad [mol\ cm^{-2}\ s^{-1}] \tag{8}$$

It is important to note that the model is strictly valid only if liquid water transport at any place in the porous layers is absent in the data used for parametrization. Therefore, firstly the temperature profile is modelled. Then, secondly the local saturation pressure is derived and compared with the simulated water partial pressure Data points, for which the local saturation pressure is reached or exceeded at any through-plane position, were neglected.

The temperature profile follows from

$$0 = k(z) \cdot \frac{d^2 T(z)}{dz^2} + H(z) \tag{9}$$

with the boundary conditions

$$T(z = z|_{T,a}) = T_{in,anode} \quad [K] \tag{10}$$
$$T(z = z|_{T,c}) = T_{in,cathode} \quad [K]$$

where $T(z = z|_{T,a/c})$ represents the temperature at the sensor position in the flow fields and the experimentally determined thermal conductivity, $k(z)$. $H(z)$ is the heat of the electrochemical reaction and Ohmic losses

$$H(z) = \begin{cases} (U_0 - U) \cdot i - R_{HFR} \cdot i^2 & CCL \\ R_{HFR} \cdot i^2 & PEM \\ 0 & MPL\&GDL \end{cases} \quad [W\ cm^{-3}] \tag{11}$$

The cell voltage, U, and high frequency resistance, R_{HFR}, are directly measured at the defined current density i. U_0 is the open circuit voltage that follows from the Nernst equation.

$$U_0 = \frac{\Delta H - T\Delta S}{n \cdot F} + \frac{R \cdot T}{n \cdot F} \cdot ln\left(\frac{p_{H_2O}}{p_{H_2} \cdot p_{o_2}^{0.5}}\right) \quad [V] \tag{12}$$

The local saturation pressure (neglecting capillary effects) follows from Eq. (1) by replacing T_{dp} with $T(z)$.

To give a visual impression of the model and its mechanics, here finally, an example of a simulation of one of the test points is presented in Fig. 3 (parameters according to Table 3). From the overall simulation regime only the excerpt representing the MEA is shown. In Fig. 3(a) the water production rate derived from the homogeneous current density profile in the CCL is presented. The related water partial pressure is shown in (e), the linked total water fluxes in (b). The absence of condensation can be verified by comparing with the saturation pressure profile (e) based on the temperature profile in (d) with the heat sources shown in (c).

4. Results and discussion

In the following, firstly experimentally measured net water fluxes are presented. Afterwards, the fitting of the membrane water transport parameters at various sets of inlet operating conditions is shown and empirical correlations between them and the water transport parameters are derived. These correlations are used to extend the model with the aim of describing membrane water transport as a function of the inlet operating conditions. Finally the sensitivity of the model is analysed with respect to the influence of dew point accuracy.

Net water flux

The net anode water flux (difference in total water flux from inlet to outlet) of two MEA samples of the same type, with the test points described in Table 1, with the nominal set of 70 °C, 2 bara and 84%RH, is shown in Fig. 4. From the amount of transported water, it can be seen firstly, that, as soon as a load is applied (see test points 7–9), the combination of electroosmotic flux and diffusion dominate the membrane water transport. At the load of 0.5 A cm^{-2} (test point 7) the net water flux is comparable to the net water flux at dew point gradients up to 10 K (test points 2 and 4). At the highest load (test point 9) the water flux is about four times higher. Secondly, in the absence of a load, the concentration gradient is the most important driving force — it dominates the test points 1–4. Thirdly, also the gas pressure gradient results in a small, but measurable water flux (test points 5–6).

Next, the plausibility of the data at 70 °C, 2 bara and 84%RH (Fig. 4) is evaluated by comparison with literature. Unfortunately, an exact quantification of the water flux differences in literature data is not possible with the information in the respective papers. In most cases, essential information is missing (conditioning and measurement time of the load points, type and accuracy of relevant sensors). In other cases, the relevant MEA components are different or not always published. Nevertheless, the data can be used to check the magnitude of the water fluxes recorded here. In Adachi et al. [26], water transport through the membrane was determined in an *ex situ* vapour/vapour measurement at 70 °C, highly saturated operating conditions and 10%RH gradients. The water flux was found to be 0.32 µmol cm^{-2} s^{-1}, which is comparable to the first anode net water flux from Fig. 4, of 0.50 µmol cm^{-2} s^{-1}. The discrepancy is plausible as in [26] a re-cast Nafion membrane (11 – 28 µm), prepared by casting an ionomer solution onto a PET film, was used, while the membrane used in our study was a commercial reinforced membrane. The data points 7–9 can be compared with the *in situ* measurement of a 25 µm thick membrane in Yau et al. [35]: Water fluxes of 1 – 4 µmol cm^{-2} s^{-1}, measured at comparable current densities, slightly different operating conditions and with an additional

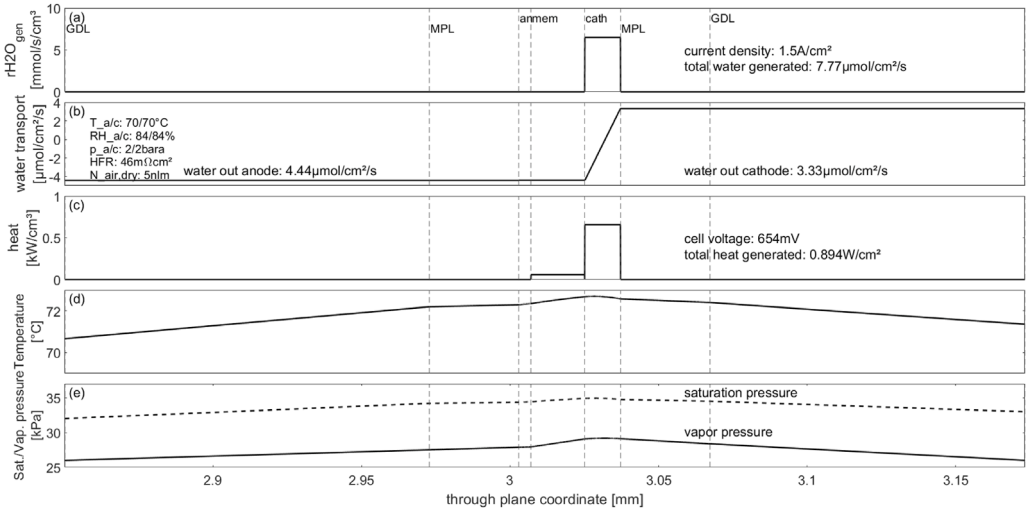

Fig. 3. Simulated through plane profiles for the test point 70 °C, 2 bara, 84%RH and 1.5 A/cm^2. Cell voltage and high frequency resistance are taken from the data set.

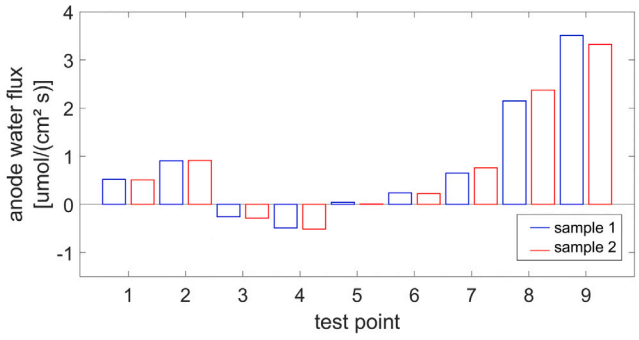

Fig. 4. Measured net anode water flux of two samples of the same MEA type at 70 °C, 2 bara and 84%RH as a function of the nine test points (for definition see Table 1).

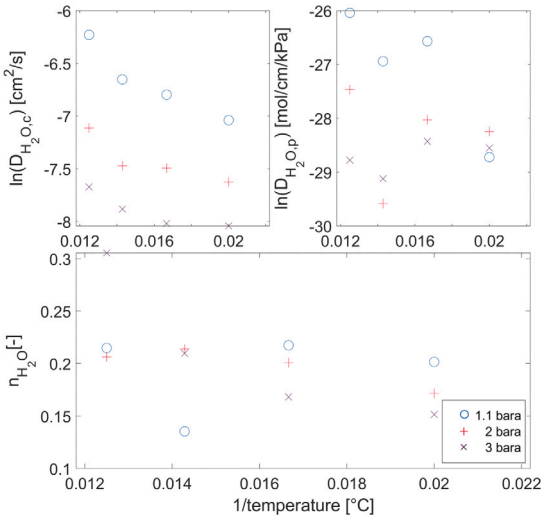

Fig. 5. Water transport parameter as a function of $1/temperature$; circles represent 1.1 bara, the cross 2 bara and the star 3 bara measurement.

humidity gradient are in line with 0.7 – 3.5 µmol cm^{-2} s^{-1} reported here. Further sources to confirm the measured water flows can be found in Yau et al. [36] and Mulyazmi et al. [51].

Model parametrization

To analyse the dependences of the nominal operation conditions at cell inlet, the model parameters $D_{H_2O,c}$, $D_{H_2O,p}$ and $n_{H_2O,i}$ are determined for of each set of operating conditions individually. Fig. 5 shows the identified parameters as a function of the nominal inlet operating conditions, as specified above (Table 1 and related text). The individually fitted data sets show the temperature and pressure dependencies of concentration-, pressure- and electroosmotic driven water transport. These were further investigated with regard to empirical correlations. The temperature dependence of $D_{H_2O,c}$ in Fig. 5 was modelled using the Arrhenius approach. From the slope, it can be deduced that the activation energy of this transport process decreases with increasing temperature. Furthermore, an inverse operation gas pressure dependence is seen for water transport, in accordance with Husar et al. [43].

$$D_{H_2O,c} = \frac{D_{c,0}}{p} \cdot exp\left(\frac{-E_{A,c}}{RT}\right) \qquad [\text{cm}^2\ \text{s}^{-1}] \quad (13)$$

The gas pressure gradient dependent water transport coefficient $D_{H_2O,p}$ in Fig. 5 does not show a clear trend. The increased noise of this parameter results from the low water transport rates of this gradient (see Fig. 4) and the associated challenges in determination. This parameter is also modelled with the help of the Arrhenius and inverse pressure approach.

$$D_{H_2O,p} = \frac{D_{p,0}}{p} \cdot exp\left(\frac{-E_{A,p}}{RT}\right) \qquad [\text{mol cm}^{-1}\ \text{kPa}^{-1}] \quad (14)$$

For the electro-osmotic drag, also no clear trend of $n_{H_2O,i}$ is found. Therefore, we used a polynomial approach for interpolation.

$$n_{H_2O,i} = D_{i0} + D_{i,T} \cdot T + D_{i,T^2} \cdot T^2 + D_{i,T^3} \cdot T^3 + D_{i,p} \cdot p \qquad [-] \quad (15)$$

The new parameters (Eq. (13)–(15)) are identified in a simultaneous fit of all experimentally measured water fluxes. The target function is:

$$res = \sqrt{\frac{1}{n-1} \cdot \left(\sum_{k=1}^{n} j_{sim,k} - \sum_{k=1}^{n} j_{exp,k}\right)^2} \quad (16)$$

During optimization it was ensured that condensation is absent in the data set underlying the parametrization. Test points showing condensation, i.e. $p_{sat} \geq p_{H_2O}$ at any through plane position z, are marked unfeasible. The parametrization is repeated until all unfeasible test points are excluded.

Table 2
Material parameters used for calculation.

Component	k_x [W cm^{-1} K^{-1}]	Porosity [1]	Tortuosity [1]	Thickness [µm]
Bipolar plate T-Sensor position	0.123	0	1	2500
Gas Diffusion Layer (GDL)	0.00313	0.692	2.41	99.2
Micro Porous Layer (MPL)	0.01 [50]	0.5	2	30
Cathode Catalyst Layer (CCL)	0.00218 [49]	0.7	2.4	12
Anode Catalyst Layer (ACL)	0.00214 [49]	0.7	2.4	4

Table 3
Transport parameters resulting from the fit.

Parameter	Value	Unit
$D_{c,0}$	12.15	cm^2 s^{-1}
$E_{A,c}$	$12.79 \cdot 10^3$	J mol^{-1}
$D_{p,0}$	$4.62 \cdot 10^{-9}$	mol cm^{-1} kPa^{-1}
$E_{A,p}$	$5.29 \cdot 10^3$	J mol^{-1}
$D_{i,0}$	$2.54 \cdot 10^{-6}$	–
$D_{i,T}$	$-4.18 \cdot 10^{-8}$	K^{-1}
D_{i,T^2}	$-1.20 \cdot 10^{-6}$	K^{-1}
D_{i,T^3}	$8.67 \cdot 10^{-9}$	K^{-1}
$D_{i,p}$	$9.35 \cdot 10^{-11}$	kPa^{-1}

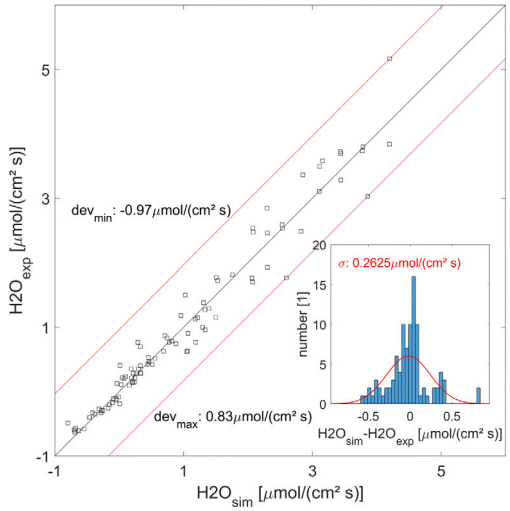

Fig. 6. Comparison of simulated net anode water removal rates (after the simultaneous fit to all experimental data) with the experimentally measured values.

The quality of the fit with the model (Eq. (1)–(16)) to the data of all sets of nominal operating conditions is presented in Fig. 6. In this scatter plot, experimental and simulated water fluxes are compared. The simulation reproduces the experimentally measured values with a maximum deviation of up to 0.97 µmol cm^{-2} s^{-1}. The histogram of the deviation is used to calculate a standard deviation of 0.26 µmol cm^{-2} s^{-1} (∼ 5% of max value). The resulting transport parameter are given in Table 3. Noteworthy, especially the smallest water fluxes have a high accuracy and only the combined water fluxes under load cause the larger inaccuracies.

In order to determine the influence of the accuracy of the dew point sensor on the transport parameters, a sensitivity analysis was carried out. Thereby, the parametrization was repeated fifty times. For each repetition the measured water fluxes were manipulated by adding random noise, reflecting the inaccuracy of the dew-point sensors. The noise was assumed to be normally-distributed with a standard deviation of 0.15 K (worst case according to the sensors data sheet), centred around the measured values. The relative deviation of the transport parameters compared with the parameters of the unaltered data set is plotted in

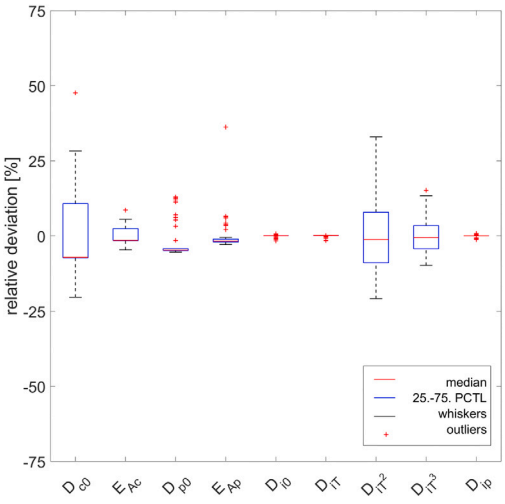

Fig. 7. Resulting relative deviation of the transport parameter caused by dew point measurement inaccuracy.

Fig. 7. The red line in the boxplot represents the median of the relative deviation, while the lower and upper edges of the box indicate the 25th and 75th percentiles, respectively. The black whiskers symbolize the most extreme parameters not considered outliers. Outliers are all results that are more than 1.5 times the interquartile range away from the 25th and 75th percentiles. The outliers are plotted using the '+' marker symbol.

With the help of this method a confidence interval of the model parameters is derived and the optimizer results are qualitatively evaluated. As discussed above, the electroosmosic water flux represents the largest contribution to the water transport from the anode. Within the parameters determining the water transport by electro-osmosis, indicated with the very low error bars, the contributions with the linear dependencies on temperature and pressure are identified most accurately. Oppositely, the parameters representing the higher orders dependencies are most vague. The next smaller water transport contribution is related to the water concentration gradient. The activation energy $E_{A,c}$ can be identified more precisely than the prefactor $D_{c,0}$. The gas pressure gradient has the smallest influence on the water transport, at the same time these parameters show a relatively high identifiability. Due to the small contribution, noise of the water transport rates do not lead to significant changes in transport parameters.

5. Conclusion

Water management is essential to achieve performance, freeze-start capability, cost and lifetime targets for fuel cell applications in passenger cars and heavy duty applications. The experimentally parametrized water transport model presented here allows calculating the total water flux as well as profiles of temperature and concentration of the specific MEA depending on the operating conditions prevailing in the flow fields.

The *in situ* water flow measurements were performed for a differential single cell with a commercially available, reinforced CCM in

combination with a GDL from Freudenberg for a range of automotive relevant operating conditions. Experimental data are validated against literature data showing good agreement. A semi-empirical model was derived and applied to the experimental data yielding explanation of water transport across the PEM in terms of individual water transport coefficients. The simulation maps the experimental measured values with a maximum deviation of 0.97 μmol cm^{-2} s^{-1} and a standard deviation of approx. 0.26 μmol cm^{-2} s^{-1} (∼ 5% of the maximum value). The uncertainty analysis shows that parameters, which represent the dominating driving forces in membrane water transport, i.e. electroosmosis and concentration gradients, are identifiable. The gas pressure gradient driven water flux, expectedly, has a small impact on the total water flux and is most difficult to be identified.

The presented approach provides a procedure for estimation of water flow rates as well as temperature and water partial pressure profiles in an operating fuel cell. The input parameters required for performance, durability or freeze start can be reliably determined, and used to assess the suitability of fuel cell components in combination with operation strategies.

List of symbols

List of symbols

Symbol	Unit
p_{H_2O}	Pa
T_{dp}	°C
T	K
$j_{H_2O}^{in/out}$	mol $cm^{-2}s^{-1}$
p^{in}	Pa
$j^{consumed}$	mol cm^{-2} s^{-1}
$D_{H_2O,c}$	cm^2 s^{-1}
$D_{H_2O,p}$	mol cm^{-1} kPa^{-1}
$n_{H_2O,i}$	–
i	A cm^{-2}
d	cm
$D_{H_2O}^{free}$	cm^2 s^{-1}
ϵ	–
τ	–
k	W cm^{-1} K^{-1}
H	W cm^{-3}
U	V
R_{HFR}	Ohm
$D_{c,0}$	cm^2 s^{-1}
$E_{A,c}$	J mol^{-1}
$D_{p,0}$	mol cm^{-1} kPa^{-1}
$E_{A,p}$	J mol^{-1}
$n_{i,0}$	–
$D_{i,T}$	K^{-1}
D_{i,T^2}	K^{-1}
D_{i,T^3}	K^{-1}
$D_{i,p}$	kPa^{-1}

CRediT authorship contribution statement

Lukas Lübben: Conceptualization, Methodology, Formal analysis, Software, Investigation, Writing – original draft. **Sebastian Kirsch:** Conceptualization, Validation, Review & Editing, Supervision. **Thomas Kadyk:** Conceptualization, Review & Editing, Supervision. **Michael Eikerling:** Conceptualization, Review & Editing, Supervision.

Declaration of competing interest

The authors declare that they have no known competing financial interests or personal relationships that could have appeared to influence the work reported in this paper.

Data availability

The authors do not have permission to share data.

References

[1] M. Eikerling, Water management in cathode catalyst layers of PEM fuel cells, J. Electrochem. Soc. 153 (3) (2006) E58, http://dx.doi.org/10.1149/1.2160435.

[2] W. Olbrich, T. Kadyk, U. Sauter, M. Eikerling, Review—Wetting phenomena in catalyst layers of PEM fuel cells: Novel approaches for modeling and materials research, J. Electrochem. Soc. 169 (5) (2022) 054521, http://dx.doi.org/10.1149/1945-7111/ac6e8b.

[3] A. Kusoglu, A.Z. Weber, New insights into perfluorinated sulfonic-acid ionomers, Chem. Rev. 117 (3) (2017) 987–1104, http://dx.doi.org/10.1021/acs.chemrev.6b00159.

[4] N. Macauley, M. Watson, M. Lauritzen, S. Knights, G.G. Wang, E. Kjeang, Empirical membrane lifetime model for heavy duty fuel cell systems, J. Power Sources 336 (2016) 240–250, http://dx.doi.org/10.1016/j.jpowsour.2016.10.068.

[5] D.R. Baker, D.A. Caulk, K.C. Neyerlin, M.W. Murphy, Measurement of oxygen transport resistance in PEM fuel cells by limiting current methods, J. Electrochem. Soc. 156 (9) (2009) B991, http://dx.doi.org/10.1149/1.3152226.

[6] M. Göbel, S. Kirsch, L. Schwarze, L. Schmidt, H. Scholz, J. Haußmann, M. Klages, J. Scholta, H. Markötter, S. Alrwashdeh, I. Manke, B.R. Müller, Transient limiting current measurements for characterization of gas diffusion layers, J. Power Sources 402 (9) (2018) 237–245, http://dx.doi.org/10.1016/j.jpowsour.2018.09.003.

[7] T. Muzaffar, T. Kadyk, M. Eikerling, Tipping water balance and the pt loading effect in polymer electrolyte fuel cells: A model-based analysis, Sustain. Energy Fuels 2 (6) (2018) 1189–1196, http://dx.doi.org/10.1039/C8SE00026C.

[8] W. Bi, Q. Sun, Y. Deng, T.F. Fuller, The effect of humidity and oxygen partial pressure on degradation of Pt/C catalyst in PEM fuel cell, Electrochim. Acta 54 (6) (2009) 1826–1833, http://dx.doi.org/10.1016/j.electacta.2008.10.008.

[9] M. Obermaier, M. Rauber, A. Bauer, T. Lochner, F. Du, C. Scheu, Local fuel starvation degradation of an automotive PEMFC full size stack, Fuel Cells 20 (4) (2020) 394–402, http://dx.doi.org/10.1002/fuce.201900180.

[10] E.L. Thompson, J. Jorne, W. Gu, H.A. Gasteiger, PEM fuel cell operation at −20 °C.: I. Electrode and membrane water (charge) storage, J. Electrochem. Soc. 155 (6) (2008) B625, http://dx.doi.org/10.1149/1.2905857.

[11] M. Eikerling, A.A. Kulikovsky, Polymer Electrolyte Fuel Cells: Physical Principles of Materials and Operation, CRC Press, Boca Raton, Florida, 2015, http://dx.doi.org/10.1201/b17429.

[12] F.J. Asensio, J.I. San Martín, I. Zamora, G. Saldaña, O. Oñederra, Analysis of electrochemical and thermal models and modeling techniques for polymer electrolyte membrane fuel cells, Renew. Sustain. Energy Rev. 113 (2019) 109283, http://dx.doi.org/10.1016/j.rser.2019.109283.

[13] W. Dai, H. Wang, X.-Z. Yuan, J.J. Martin, D. Yang, J. Qiao, J. Ma, A review on water balance in the membrane electrode assembly of proton exchange membrane fuel cells, Int. J. Hydrogen Energy 34 (23) (2009) 9461–9478, http://dx.doi.org/10.1016/j.ijhydene.2009.09.017.

[14] E.J.F. Dickinson, G. Smith, Modelling the proton-conductive membrane in practical polymer electrolyte membrane fuel cell (PEMFC) simulation: A review, Membranes 10 (11) (2020) http://dx.doi.org/10.3390/membranes10110310.

[15] T.E. Springer, T.A. Zawodzinski, S. Gottesfeld, Polymer electrolyte fuel cell model, J. Electrochem. Soc. 138 (8) (1991) 2334–2342, http://dx.doi.org/10.1149/1.2085971.

[16] D.M. Bernardi, M.W. Verbrugge, Mathematical model of a gas diffusion electrode bonded to a polymer electrolyte, AIChE J. 37 (8) (1991) 1151–1163, http://dx.doi.org/10.1002/AIC.690370805.

[17] T.F. Fuller, J. Newman, Water and thermal management in solid–polymer–electrolyte fuel cells, J. Electrochem. Soc. 140 (5) (1993) 1218–1225, http://dx.doi.org/10.1149/1.2220960.

[18] S. Um, C.-Y. Wang, K.S. Chen, Computational fluid dynamics modeling of proton exchange membrane fuel cells, J. Electrochem. Soc. 147 (12) (2000) 4485, http://dx.doi.org/10.1149/1.1394090.

[19] S. Mazumder, J.V. Cole, Rigorous 3-D mathematical modeling of PEM fuel cells, J. Electrochem. Soc. 150 (11) (2003) A1510, http://dx.doi.org/10.1149/1.1615609.

[20] M. Eikerling, Y.I. Kharkats, A.A. Kornyshev, Y.M. Volfkovich, Phenomenological theory of electro–osmotic effect and water management in polymer electrolyte proton–conducting membranes, J. Electrochem. Soc. 145 (8) (1998) 2684–2699, http://dx.doi.org/10.1149/1.1838700.

[21] A.Z. Weber, J. Newman, Transport in polymer-electrolyte membranes, J. Electrochem. Soc. 151 (2) (2004) A311, http://dx.doi.org/10.1149/1.1639157.

[22] G.J.M. Janssen, A phenomenological model of water transport in a proton exchange membrane fuel cell, J. Electrochem. Soc. 148 (12) (2001) A1313, http://dx.doi.org/10.1149/1.1415031.

[23] P.W. Majsztrik, M.B. Satterfield, A.B. Bocarsly, J.B. Benziger, Water sorption, desorption and transport in Nafion membranes, J. Membr. Sci. 301 (1–2) (2007) 93–106, http://dx.doi.org/10.1016/j.memsci.2007.06.022.

[24] M.H. Eikerling, P. Berg, Poroelectroelastic theory of water sorption and swelling in polymer electrolyte membranes, Soft Matter 7 (13) (2011) 5976, http://dx.doi.org/10.1039/c1sm05273j.
[25] D.A. Caulk, D.R. Baker, Heat and water transport in hydrophobic diffusion media of PEM fuel cells, J. Electrochem. Soc. 157 (8) (2010) B1237, http://dx.doi.org/10.1149/1.3454721.
[26] M. Adachi, T. Navessin, Z. Xie, F.H. Li, S. Tanaka, S. Holdcroft, Thickness dependence of water permeation through proton exchange membranes, J. Membr. Sci. 364 (1–2) (2010) 183–193, http://dx.doi.org/10.1016/j.memsci.2010.08.011.
[27] A.Z. Weber, J. Newman, Effects of microporous layers in polymer electrolyte fuel cells, J. Electrochem. Soc. 152 (4) (2005) A677, http://dx.doi.org/10.1149/1.1861194.
[28] J. Zhou, S. Shukla, A. Putz, M. Secanell, Analysis of the role of the microporous layer in improving polymer electrolyte fuel cell performance, Electrochim. Acta 268 (4) (2018) 366–382, http://dx.doi.org/10.1016/j.electacta.2018.02.100.
[29] X. Ye, C.-Y. Wang, Measurement of water transport properties through membrane-electrode assemblies: Part1, J. Electrochem. Soc. 154 (7) (2007) B676, http://dx.doi.org/10.1149/1.2737379.
[30] Q. Yan, H. Toghiani, J. Wu, Investigation of water transport through membrane in a PEM fuel cell by water balance experiments, J. Power Sources 158 (1) (2006) 316–325, http://dx.doi.org/10.1016/j.jpowsour.2005.09.013.
[31] J.P. Owejan, J.E. Owejan, W. Gu, T.A. Trabold, T.W. Tighe, M.F. Mathias, Water transport mechanisms in PEMFC gas diffusion layers, J. Electrochem. Soc. 157 (10) (2010) B1456, http://dx.doi.org/10.1149/1.3468615.
[32] E. Misran, N.S.M. Hassan, W.R.W. Daud, E.H. Majlan, M.I. Rosli, Water transport characteristics of a PEM fuel cell at various operating pressures and temperatures, Int. J. Hydrogen Energy 38 (22) (2013) 9401–9408, http://dx.doi.org/10.1016/j.ijhydene.2012.12.076.
[33] V. Liso, S. Simon Araya, A.C. Olesen, M.P. Nielsen, S.K. Kær, Modeling and experimental validation of water mass balance in a PEM fuel cell stack, Int. J. Hydrogen Energy 41 (4) (2016) 3079–3092, http://dx.doi.org/10.1016/j.ijhydene.2015.10.095.
[34] K. Chadha, S. Martemianov, A. Thomas, Estimation of the effective water diffusion coefficient in Nafion ® membrane by water balance measurements, Fuel Cells 21 (2) (2021) 139–148, http://dx.doi.org/10.1002/fuce.202000150.
[35] T.C. Yau, P. Sauriol, X.T. Bi, J. Stumper, Experimental determination of water transport in polymer electrolyte membrane fuel cells, J. Electrochem. Soc. 157 (9) (2010) B1310, http://dx.doi.org/10.1149/1.3456621.
[36] T.C. Yau, M. Cimenti, X. Bi, J. Stumper, Effects of cathode gas diffusion layer design on polymer electrolyte membrane fuel cell water management and performance, J. Power Sources 196 (22) (2011) 9437–9444, http://dx.doi.org/10.1016/j.jpowsour.2011.07.002.
[37] Zawodzinski, Water uptake by and transport through nation—117 membranes, J. Electrochem. Soc. 1993 (140) (1993) 1041–1047.
[38] T.F. Fuller, J. Newman, Experimental determination of the transport number of water in Nafion 117 membrane, J. Electrochem. Soc. 139 (5) (1992) 1332–1337, http://dx.doi.org/10.1149/1.2069407.
[39] R. Shimokawa, H. Nagai, Y. Sugesawa, H. Minakuchi, M. Sudoh, Real time measurement of water transport in polymer electrolyte fuel cell, ECS Trans. 58 (1) (2013) 1659–1668, http://dx.doi.org/10.1149/05801.1659ecst.
[40] M.J. Cheah, I.G. Kevrekidis, J. Benziger, Effect of interfacial water transport resistance on coupled proton and water transport across Nafion, J. Phys. Chem. B 115 (34) (2011) 10239–10250, http://dx.doi.org/10.1021/jp204785t.
[41] Q. Dong, J. Kull, M.M. Mench, Real-time water distribution in a polymer electrolyte fuel cell, J. Power Sources 139 (1–2) (2005) 106–114, http://dx.doi.org/10.1016/j.jpowsour.2004.06.068.
[42] B. Kientiz, H. Yamada, N. Nonoyama, A.Z. Weber, Interfacial water transport effects in proton-exchange membranes, J. Fuel Cell Sci. Technol. 8 (1) (2011) 4679, http://dx.doi.org/10.1115/1.4002398.
[43] A. Husar, A. Higier, H. Liu, In situ measurements of water transfer due to different mechanisms in a proton exchange membrane fuel cell, J. Power Sources 183 (1) (2008) 240–246, http://dx.doi.org/10.1016/j.jpowsour.2008.04.042.
[44] T. Kim, S. Lee, H. Park, A study of water transport as a function of the microporous layer arrangement in PEMFCs, Int. J. Hydrogen Energy 35 (16) (2010) 8631–8643, http://dx.doi.org/10.1016/j.ijhydene.2010.05.123.
[45] G. Janssen, M. Overvelde, Water transport in the proton-exchange-membrane fuel cell: Measurements of the effective drag coefficient, J. Power Sources 101 (1) (2001) 117–125, http://dx.doi.org/10.1016/S0378-7753(01)00708-X.
[46] A. Thomas, G. Maranzana, S. Didierjean, J. Dillet, O. Lottin, Measurements of electrode temperatures, heat and water fluxes in PEMFCs: Conclusions about transfer mechanisms, J. Electrochem. Soc. 160 (2) (2012) F191–F204, http://dx.doi.org/10.1149/2.006303jes.
[47] K. Christmann, K.A. Friedrich, N. Zamel, Activation mechanisms in the catalyst coated membrane of PEM fuel cells, Prog. Energy Combust. Sci. 85 (11) (2021) 100924, http://dx.doi.org/10.1016/j.pecs.2021.100924.
[48] E. Balogun, A.O. Barnett, S. Holdcroft, Cathode starvation as an accelerated conditioning procedure for perfluorosulfonic acid ionomer fuel cells, J. Power Sources Adv. 3 (2020) 100012, http://dx.doi.org/10.1016/j.powera.2020.100012.
[49] M. Ahadi, M. Tam, M.S. Saha, J. Stumper, M. Bahrami, Thermal conductivity of catalyst layer of polymer electrolyte membrane fuel cells: Part 1 – Experimental study, J. Power Sources 354 (2017) 207–214, http://dx.doi.org/10.1016/j.jpowsour.2017.02.016.
[50] H. Scholz, Modellierung und Untersuchung von Flutungsphänomenen in Niedertemperatur-PEM-Brennstoffzellen (Dissertation), 2015.
[51] Mulyazmi, W. Daud, E.H. Majlan, M.I. Rosli, Water balance for the design of a PEM fuel cell system, Int. J. Hydrogen Energy 38 (22) (2013) 9409–9420, http://dx.doi.org/10.1016/j.ijhydene.2012.12.014.